

## General relativistic treatment of *f*-mode oscillations of hyperonic stars

Bikram Keshari Pradhan \* and Debarati Chatterjee †

Inter-University Centre for Astronomy and Astrophysics, Pune University Campus, Pune 411007, India

Michael Lanoye  and Prashanth Jaikumar 

Department of Physics and Astronomy, California State University Long Beach, Long Beach, California 90840, USA



(Received 1 February 2022; accepted 29 June 2022; published 28 July 2022)

We present a systematic study of *f*-mode oscillations in neutron stars containing hyperons, extending recent results obtained within the Cowling approximation to linearized general relativity. Employing a relativistic mean-field model, we find that the Cowling approximation can overestimate the quadrupolar *f*-mode frequency of neutron stars by up to 30% compared to the frequency obtained in the linearized general relativistic formalism. Imposing current astrophysical constraints, we derive updated empirical relations for gravitational wave asteroseismology. The frequency and damping time of quadrupole *f*-mode oscillations of hyperonic stars are found to be in the range of 1.47–2.45 kHz and 0.13–0.51 s, respectively. Our correlation studies demonstrate that among the various parameters of the nucleonic and hyperonic sectors of the model, the nucleon effective mass shows the strongest correlation with mode characteristics and neutron star observables. Estimates for the detectability of *f* modes in a transient burst of gravitational waves from isolated hyperonic stars is also provided.

DOI: [10.1103/PhysRevC.106.015805](https://doi.org/10.1103/PhysRevC.106.015805)

### I. INTRODUCTION

Neutron stars (NS) are natural laboratories to probe the behavior of matter under extreme conditions, such as ultra high densities, rapid rotation, or ultrastrong magnetic fields [1–3]. With the interior composition of the NS core uncertain, it is conjectured that strangeness in the form of hyperons, meson condensates, or even deconfined quark matter may appear at such high densities, which can affect several NS observable properties. For example, the appearance of hyperons can affect NS maximum mass, radius, cooling, or gravitational wave (GW) emission from unstable quasinormal modes [4], and one can then look for the signatures of such exotic matter in NS observables.

A good theoretical model of NS should be able to explain basic NS astrophysical observables, such as its mass or radius. In order to connect the NS internal composition with these global properties, one requires an equation of state (EoS). Various EoS models exist that employ *ab initio* many-body methods or phenomenological theories in order to extrapolate baryon-baryon interaction to densities or neutron-proton asymmetries relevant for describing NS matter. Among the different EoS models, one class of realistic phenomenological models is based on the relativistic mean field (RMF) approach, which is a particular self-consistent approximation to in-medium nuclear many-body forces and contains density-dependent parameters that are fit to nuclear experimental observables [5,6]. In this work, we adopt one such

RMF model as a representative of this class of EoS and call it simply “the RMF model.”

With the current generation of space-based and ground-based telescopes, neutron stars are observed at multiple wavelengths of the electromagnetic spectrum from radio to x-rays to gamma rays. For neutron stars in a binary, post-Keplerian effects allow the component masses to be determined to high accuracy [7–11]. Radius measurements that rely solely on thermal emission from the NS surface suffer from several uncertainties and cannot be determined with high precision. However, the recently launched Neutron Star Interior Composition Explorer (NICER) mission [12] has improved radius determination by employing novel techniques to study pulse modulation profiles, which enables up to 5% accuracy in the determination of the radius [13,14].

In addition to electromagnetic emission, neutron stars can also act as sources of GWs. Any nonaxisymmetric perturbation or a merger of neutron stars in a binary can produce copious amounts of GWs. In the case of mergers, the tidal deformation of a component NS under the strong gravitational force of the other can constrain the properties of matter in the interior [15–18]. Recent detections of NS-NS (BNS) collisions (GW170817) or NS-BH mergers (GW200105 and GW200115) by the LIGO-Virgo-KAGRA collaboration of GW detectors have opened up new frontiers in multimessenger astronomy [19].

In the context of GW, the secular quasinormal modes (QNM) of NS are particularly interesting, since they carry information about the interior composition and viscous forces that damp these modes. QNMs in neutron stars are categorized by the restoring force that bring the perturbed star back to equilibrium [20–22]. Examples include the fundamental

\*bikramp@iucaa.in

†debarati@iucaa.in

$f$  mode,  $p$  modes, and  $g$  modes (driven by pressure and buoyancy respectively), as well as  $r$  modes (Coriolis force) and pure space-time  $w$  modes. Several of these modes are expected to be excited during SN explosions [23], or in a starquake [24] or in isolated perturbed NSs [25], or during the post-merger phase of a binary NS [26–28], with the  $f$  mode being the primary target of interest. It has been argued that spin and eccentricity enhance the excitation of the  $f$  modes during the inspiral phase of NS mergers [29,30]. The fundamental  $f$  modes are within the sensitivity range of current generation of GW detectors and are correlated with the tidal deformability during the inspiral phase of NS mergers [31–34]. The  $g$  modes can be excited during inspiral of a merger event [34] and are also sensitive to the internal composition of NS [35,36]. However, the impact on GW is too weak to be noticed by the current generation of instruments [34]. Which leads us to focus on  $f$  mode oscillation of NS.

Among the many studies in the literature that study the  $f$  mode, the pioneering work of Andersson and Kokkotas [37,38] relating the NS global properties such as mass, radius, or compactness with the frequency and damping times of QNMs is the most relevant motivation to our work. However, the majority of these studies rely on the Cowling approximation (neglecting perturbations of the background metric), instead of calculating in full general relativity (GR). While the Cowling approximation is justified as a first reasonable estimate of the mode frequency, full GR is required for a more accurate computation of the mode frequency and to find the damping time in order to extract reliable information about the NS EoS from GW data.

In a recent study [39], we performed a systematic investigation of the role of nuclear saturation parameters on the oscillation modes for a purely nucleonic nonrotating NS in the framework of the RMF model. We then extended this investigation [40] to study the effect of the appearance of hyperons on the  $f$ -mode frequencies. Completing the analysis, in this work, we present the results of calculations of  $f$  modes of hyperonic stars in a fully general relativistic framework.

This paper is organized in the following way. In Sec. II, we discuss the RMF model Lagrangian and the model's parameters. In Sec. III, the resulting macroscopic properties of the NS are presented, followed by Sec. IV detailing the GR equations used to determine the global  $f$ -mode frequency. We compile our results in Sec. V and summarize our conclusions in Sec. VI.

## II. MICROSCOPIC MODEL FOR THE EQUATION OF STATE

### A. The relativistic mean-field model

The charge-neutral,  $\beta$ -equilibrated matter in the NS interior is described by our chosen RMF theory, which provides a Lorentz covariant description of the microphysics of the NS interior. In the RMF model, baryon-baryon interaction is mediated by the exchange of scalar ( $\sigma$ ), vector ( $\omega$ ), and isovector ( $\rho$ ) mesons, while hyperon-hyperon interactions are mediated by additional strange scalar ( $\sigma^*$ ) and strange vector ( $\phi$ ) mesons [41]. The interaction Lagrangian density ( $\mathcal{L}$ ) can

be written as

$$\begin{aligned} \mathcal{L} = & \sum_B \bar{\psi}_B (i\gamma^\mu \partial_\mu - m_B + g_{\sigma B} \sigma - g_{\omega B} \gamma_\mu \omega^\mu \\ & - g_{\rho B} \gamma_\mu \vec{I}_B \cdot \vec{\rho}^\mu) \psi_B + \frac{1}{2} (\partial_\mu \sigma \partial^\mu \sigma - m_\sigma^2 \sigma^2) - U_\sigma \\ & + \frac{1}{2} m_\omega^2 \omega_\mu \omega^\mu - \frac{1}{4} \omega_{\mu\nu} \omega^{\mu\nu} - \frac{1}{4} (\vec{\rho}_{\mu\nu} \cdot \vec{\rho}^{\mu\nu} - 2m_\rho^2 \vec{\rho}_\mu \cdot \vec{\rho}^\mu) \\ & + \Lambda_\omega (g_{\rho N}^2 \vec{\rho}_\mu \cdot \vec{\rho}^\mu) (g_{\omega N}^2 \omega_\mu \omega^\mu) + \mathcal{L}_{YY} + \mathcal{L}_\ell, \end{aligned} \quad (1)$$

where

$$\begin{aligned} U_\sigma &= \frac{1}{3} b m_N (g_{\sigma N} \sigma)^3 + \frac{1}{4} c (g_{\sigma N} \sigma)^4, \\ \mathcal{L}_{YY} &= \sum_Y \bar{\psi}_Y (g_{\sigma^* Y} \sigma^* - g_{\phi Y} \gamma_\mu \phi^\mu) \psi_Y + \frac{1}{2} m_\phi^2 \phi_\mu \phi^\mu \\ & - \frac{1}{4} \phi_{\mu\nu} \phi^{\mu\nu} + \frac{1}{2} (\partial_\mu \sigma^* \partial^\mu \sigma^* - m_{\sigma^*}^2 \sigma^{*2}), \\ \mathcal{L}_\ell &= \sum_{\ell=\{e^-, \mu^-\}} \bar{\psi}_\ell (i\gamma^\mu \partial_\mu - m_\ell) \psi_\ell. \end{aligned}$$

The governing field equations for constituent baryons and mesons can be found in our previous work [40]. In the mean-field approximation, meson fields are replaced by their ground-state expectation values. Replacing the nonvanishing mean-meson expectation components as [5] “ $\bar{\sigma} = \langle \sigma \rangle$ ,  $\bar{\omega}_0 = \langle \omega_0 \rangle$ ,  $\bar{\rho}_{03} = \langle \rho_{03} \rangle$ ,  $\bar{\sigma}^* = \langle \sigma^* \rangle$ ,  $\bar{\phi}_0 = \langle \phi_0 \rangle$ ,” the energy density for the given Lagrangian density (1) is given by [40]:

$$\begin{aligned} \epsilon = & \frac{1}{2} m_\sigma^2 \bar{\sigma}^2 + \frac{1}{2} m_{\sigma^*}^2 \bar{\sigma}^{*2} + \frac{1}{2} m_\omega^2 \bar{\omega}_0^2 + \frac{1}{2} m_\rho^2 \bar{\rho}_{03}^2 \\ & + \frac{1}{2} m_\phi^2 \bar{\phi}_0^2 + \frac{1}{3} b m_N (g_{\sigma N} \bar{\sigma})^3 + \frac{1}{4} c (g_{\sigma N} \bar{\sigma})^4 \\ & + \sum_B \frac{g_{sB}}{2\pi^2} \int_0^{k_{FB}} \sqrt{k^2 + m_B^{*2}} dk \\ & + 3\Lambda_\omega (g_{\rho N} g_{\omega N} \bar{\rho}_{03} \bar{\omega}_0)^2 \\ & + \sum_\ell \frac{g_{s\ell}}{2\pi^2} \int_0^{k_{F\ell}} \sqrt{k^2 + m_\ell^2} dk, \end{aligned} \quad (2)$$

where  $g_{si}$  and  $k_{Fi}$  represent spin degeneracy and Fermi momentum of  $i$ th species, respectively.  $m_B^*$  is the effective mass for baryon  $B$  and given by

$$m_B^* = m_B - g_{\sigma B} \bar{\sigma} - g_{\sigma^* B} \bar{\sigma}^*. \quad (3)$$

The pressure ( $p$ ) is given by the Gibbs-Duhem relation [6],

$$p = \sum_{i=B,\ell} \mu_i n_i - \epsilon, \quad (4)$$

with  $n_i$  and  $\mu_i$  as the number density and chemical potential of the  $i$ th constituent, respectively. The baryon and lepton chemical potentials can be expressed respectively as

$$\begin{aligned} \mu_B &= \sqrt{k_{FB}^2 + m_B^{*2}} + g_{\omega B} \bar{\omega}_0 + g_{\phi B} \bar{\phi}_0 + I_{3B} g_{\rho B} \bar{\rho}_{03}, \\ \mu_\ell &= \sqrt{k_{F\ell}^2 + m_\ell^2}. \end{aligned} \quad (5)$$

TABLE I. Range of saturation nuclear parameters used in this work. Masses of mesons and the nucleon are fixed as  $m_\sigma = 550$  MeV,  $m_\omega = 783$  MeV,  $m_\rho = 770$  MeV,  $m_{\sigma^*} = 975$  MeV,  $m_\phi = 1020$  MeV, and  $m_N = 939$  MeV. For the masses of the hyperons, we use data from Ref. [42].

Model	$n_0$ (fm $^{-3}$ )	$E_{\text{sat}}$ (MeV)	$K$ (MeV)	$J$ (MeV)	$L$ (MeV)	$m^*/m_N$
RMF [6]	0.15–0.16	$-15.5 \pm 0.5$	230–280	$32 \pm 2$	$50 \pm 10$	$0.65 \pm 0.10$

## B. Parameters of the RMF model

### 1. Nucleon couplings

Here we briefly discuss the coupling constants, which may be regarded as model parameters. The nucleon isoscalar coupling constants ( $g_{\sigma N}$ ,  $g_{\omega N}$ ,  $b$ ,  $c$ ) are set by fixing nuclear saturation properties: nuclear saturation density ( $n_0$ ), binding energy per nucleon ( $E/A$  or  $E_{\text{sat}}$ ), incompressibility ( $K$ ), and the effective nucleon mass ( $m^*$ ) at saturation. The isovector coupling constants ( $g_{\rho N}$ ,  $\Lambda_\omega$ ) are obtained by fixing the symmetry energy ( $J$ ) and its slope ( $L$ ) at saturation [5,6]. It was concluded that in RMF models the stiffness of the EoS is mainly controlled by  $m^*$  [6]. We consider a reasonable range of  $m^*$  such that the maximum mass is above the observed limit ( $m^* < 0.75$ ) and does not induce the appearance of instabilities in the neutron matter EoS ( $m^* > 0.55$ ) [6]. The effect of astrophysical constraints on  $m^*$  is discussed in detail at the end of Sec. III. The range of saturation nuclear parameters considered in this work have been summarized in Table I.

### 2. Hyperon couplings

RMF models with attractive hyperon-hyperon interaction (mediated by the strange meson  $\sigma^*$ ) are incompatible with the current highest observed NS mass [43]. Thus, we exclude the attractive hyperon-hyperon interaction. The nonstrange scalar-hyperon couplings ( $g_{\sigma Y}$ ) are fitted to available hyperon-nucleon potential depth in normal nuclear matter [ $U_Y^N(n_0)$ ] using Eq. (6) [41,43] and the vector and isovector hyperon couplings ( $g_{\omega Y}$ ,  $g_{\rho Y}$ ,  $g_{\phi Y}$ ) are fixed to their theoretical values using the symmetries of the SU(6) quark model summarized in Refs. [41,43],

$$U_Y^N(n_0) = -g_{\sigma Y}\bar{\sigma} + g_{\omega Y}\bar{\omega}_0. \quad (6)$$

$$\begin{aligned} g_{\omega \Lambda} &= g_{\omega \Sigma} = 2g_{\omega \Xi} = \frac{2}{3}g_{\omega N}, \\ g_{\rho N} &= g_{\rho \Xi} = \frac{1}{2}g_{\rho \Sigma} \quad g_{\rho \Lambda} = 0, \\ 2g_{\phi \Lambda} &= 2g_{\phi \Sigma} = g_{\phi \Xi} = \frac{-2\sqrt{2}}{3}g_{\omega N}. \end{aligned} \quad (7)$$

Among the nucleon-hyperon potentials  $U_Y^N$ , the best known potential depth is that of  $\Lambda$ ,  $U_\Lambda^N(n_0) = -30$  MeV [44,45]. Although there is an uncertainty in  $U_\Sigma^N$ , it has been concluded from experiments that  $U_\Sigma^N$  is repulsive [45–48]. We fix the  $U_\Sigma^N$  potential to its most commonly adopted value +30 MeV. However, the value of  $U_\Xi^N$  is attractive and highly uncertain [47,49,50]. So we vary the value of  $U_\Xi^N$  within the range of -40 MeV to +40 MeV for our investigation. Once all the coupling constants for a fixed parameters set are determined,

the EoS can be evaluated for the Lagrangian given in Eq. (1). Each of the saturation parameters is randomly drawn from a uniform distribution defined in the range of the corresponding parameter as given in Table I. After applying the astrophysical constraints ( $M_{\text{max}} \geq 2M_\odot$  and tidal deformability constraint from GW170817 [18]), we are left with approximately 1500 (1483 to be exact) microscopic models for pure nucleonic matter and 1000 (1123 to be exact) microscopic models for neutron stars with nucleon-hyperon matter. For providing the asterosismolgy relations in Sec. V, we have obtained  $f$ -mode characteristics for  $2.5 \times 10^5$  neutron star.

## III. MACROSCOPIC FEATURES OF THE NEUTRON STAR

After the EoS is specified, the macroscopic structure of the NS can be described by solving the Tolman-Oppenheimer-Volkoff (TOV) equations. Starting with general spherically symmetric metric (8), the equations describing hydrostatic equilibrium (TOV) are given by Eqs. (9) and (10) and the equations governing metric functions  $\Phi(r)$  and  $\lambda(r)$  by Eqs. (11) and (12).

$$ds^2 = -e^{2\Phi(r)}dt^2 + e^{2\lambda(r)}dr^2 + r^2d\theta^2 + r^2\sin^2\theta d\phi^2, \quad (8)$$

$$\frac{dm(r)}{dr} = 4\pi r^2\epsilon(r), \quad (9)$$

$$\frac{dp(r)}{dr} = -[p(r) + \epsilon(r)]\frac{m(r) + 4\pi r^3 p(r)}{r[r - 2m(r)]}, \quad (10)$$

$$\frac{d\Phi(r)}{dr} = \frac{-1}{\epsilon(r) + p(r)}\frac{dp}{dr}, \quad (11)$$

$$e^{2\lambda(r)} = \frac{r}{r - 2m(r)}. \quad (12)$$

Integration of TOV equations for a given EoS [ $p = p(\epsilon)$ ] from the center to the surface with vanishing pressure at the surface  $p(R) = 0$  provides the stellar radius  $R$  and mass  $M = m(R)$  for equilibrium stellar models. Another boundary condition is that at the surface,  $\Phi(R) = \frac{1}{2}\log(1 - \frac{2M}{R})$ . The tidal love number  $k_2$  for a given EoS can be evaluated by solving a set of additional differential equations along with TOV equations [51], which then lead to determination of another important observable quantity, the dimensionless tidal deformability ( $\bar{\Lambda}$ )

$$\bar{\Lambda} = \frac{2}{3}k_2\left(\frac{R}{M}\right)^5. \quad (13)$$

We display the EoSs and corresponding mass-radius relations used in this work in Fig. 1 and Fig. 2, respectively. Of the EoSs obtained by randomly varying the saturation parameters in Table I, we only consider those which are compatible with recent astrophysical observational constraints, i.e., the

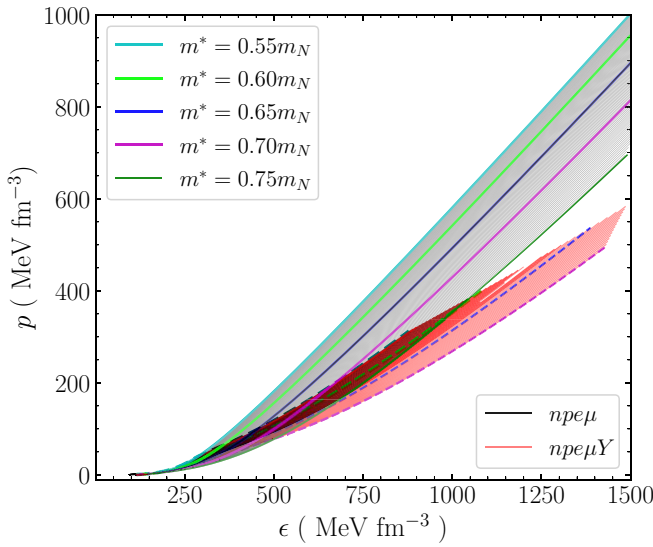


FIG. 1. EoSs used in this work. To avoid cluttering we have displayed here a few of the EoSs with nucleons (solid black lines,  $npe\mu$ ) as well as models with hyperons (solid red lines,  $npe\mu Y$ ) corresponding to the parameter space explained in Sec. II B. Specific solid (dashed) lines are shown for different effective mass for nucleonic (hyperonic) EoSs with other parameters fixed at  $n_0 = 0.150 \text{ fm}^{-3}$ ,  $E_{\text{sat}} = -16.0 \text{ MeV}$ ,  $J = 32 \text{ MeV}$ ,  $L = 60 \text{ MeV}$ ,  $K = 240 \text{ MeV}$ , and  $U_{\Xi} = -18 \text{ MeV}$ .

EoS must reproduce the maximum observed neutron star of  $2M_{\odot}$  mass and also be compatible with the tidal deformability estimation from the merger event GW170817 [18]. The dominant parameter controlling the stiffness of the EoS is

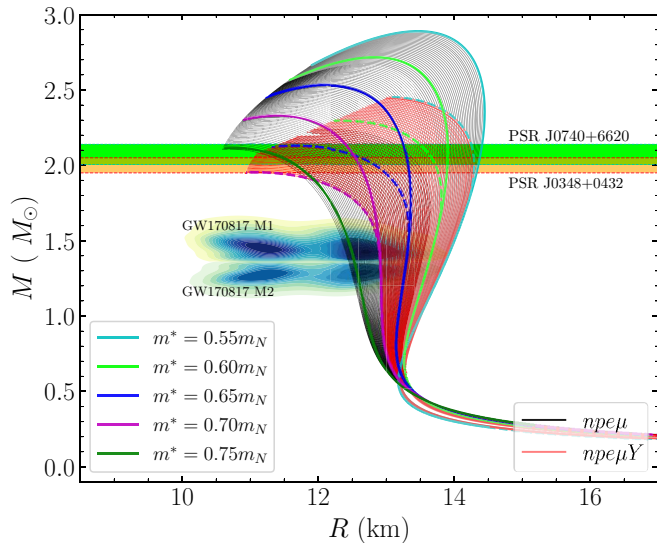


FIG. 2. Mass-radius relation corresponding to EoSs used in this work (see Fig. 1). Horizontal bands correspond to masses  $M = 2.072_{-0.066}^{+0.067} M_{\odot}$  of PSR J0740+6620 [11] (green band) and  $M = 2.01_{-0.04}^{+0.04} M_{\odot}$  of PSR J0348 + 0432 [8] (yellow band). The mass radius estimates of the two companion neutron stars in the merger event GW170817 [17] are shown by shaded area labeled with GW170817 M1 (M2) [52].

found to be the nuclear effective mass  $m^*$  [39], and its range may be constrained by the maximum observed mass and compactness [53]. We note here that while considering models with nucleonic matter, the maximum  $2M_{\odot}$  limit does not put any constraint on the uncertainty of  $m^*$  while imposing the constraint of an upper limit of tidal deformability coming from GW170817 [18] allows us to put a tight constraint on the lower limit,  $m^* > 0.60m_N$ . In the case of models with hyperonic EoSs, the maximum  $2M_{\odot}$  puts a constraint on the upper limit  $m^* \leq 0.70m_N$  along with the lower limit constraint  $m^* > 0.60m_N$  from the upper limit of tidal deformability coming from GW170817. We found that EoS models satisfying the tidal deformability constraint from event GW170817 also satisfy NS radius constraint resulting from recent NICER observations [13,14].

#### IV. CALCULATION OF OSCILLATION MODES

The theory of perturbed NSs, emitting GWs at the characteristic frequency of its QNM, was introduced in a paper by Thorne and Campolattaro in 1967 [22]. Many works [54,55], including our previous work [40], use the simplification defined by the relativistic Cowling approximation, where background metric perturbations are neglected. Frequencies obtained using the Cowling approximation for fundamental modes ( $f$  modes) are purely real and differ by 20–30% compared to frequencies obtained from the linearized equations of general relativity [56]. The Cowling approximation precludes a calculation of the damping time of QNMs. To obtain solutions in the fully general relativistic framework, different methods such as resonance matching (developed by Thorne [57] and later by Chandrasekhar [58]), direct integration [59,60], and the method of continued fractions [61,62] have been applied.

Complicating effects like rotation are essential for describing a realistic astrophysical scenario. Recent efforts suggest that the leading-order spin correction to the mode frequency is  $0.2 (\nu_s/\nu_K)$  [63] ( $\nu_s$  is the spin frequency and  $\nu_K$  is the Kepler frequency). Almost all glitching pulsars have a low spin frequency ( $\nu_s < 100 \text{ Hz}$ ). In contrast, the Kepler frequency is  $\sim 1 \text{ kHz}$ , such that they would have  $f$ -mode frequency correction  $< 2\%$ , this implies that the rotation has a minor effect on a detection event from transient NS  $f$  modes from glitching pulsars. For a merger scenario, recent efforts are going on to include the impact of  $f$ -mode dynamical tides and the spin effect on NS  $f$ -mode dynamical tide [30]. A recent article [64] concludes that the spin correction to  $f$  modes has a considerable impact on the gravitation wave for rapidly rotating stars. However, the effect of rotation is still a matter of investigation.

In this article, we employ the procedure developed by Lindblom and Detweiler (hereafter called LD) [59,60] for finding the QNMs of the  $f$  modes for nonrotating NSs. In short, the perturbation equations are solved inside the star with appropriate boundary conditions. Then a search for the complex QNM frequency ( $\omega$ ) is carried out for which one has only outgoing GWs at infinity. The real part [ $\text{Re}(\omega)$ ] of the obtained complex QNM frequency relates to the QNM frequency( $f$ ) as  $\text{Re}(\omega) = 2\pi f$ , and the imaginary part

represents the reciprocal of the damping time ( $\frac{1}{\tau_f}$ ), i.e., the obtained QNM frequency ( $\omega$ ) has the form,  $\omega = 2\pi f + i\frac{1}{\tau_f}$ . In this section, we present the basic equations that need to be solved for finding the complex QNM frequencies.

### 1. Perturbations inside the star

The perturbed metric ( $ds_p^2$ ) can be written as [22]

$$ds_p^2 = ds^2 + h_{\mu\nu}dx^\mu dx^\nu. \quad (14)$$

Following the arguments given in Thorne and Campolattaro [22], we focus on the even-parity (polar) perturbations for which the the GW and matter perturbations are coupled. Then  $h_{\mu\nu}$  can be expressed as [22,62]

$$h_{\mu\nu} = \begin{pmatrix} r^l He^{2\Phi} & i\omega r^{l+1} H_1 & 0 & 0 \\ i\omega r^{l+1} H_1 & r^l He^{2\lambda} & 0 & 0 \\ 0 & 0 & r^{l+2} K & 0 \\ 0 & 0 & 0 & r^{l+2} K \sin^2 \theta \end{pmatrix} Y_m^l e^{i\omega t}, \quad (15)$$

where  $Y_m^l$  are spherical harmonics and  $H$ ,  $H_1$ , and  $K$  are perturbed metric functions and vary with  $r$  [i.e.,  $H = H(r)$ ,  $H_1 = H_1(r)$ ,  $K = K(r)$ ]. The Lagrangian displacement vector  $\zeta = (\zeta^r, \zeta^\theta, \zeta^\phi)$  associated with the polar perturbations of the fluid can be characterized as [60,65]

$$\begin{aligned} \zeta^r &= \frac{r^l}{r} e^{-\lambda} W(r) Y_m^l e^{i\omega t} \\ \zeta^\theta &= \frac{-r^l}{r^2} V(r) \frac{\partial Y_m^l}{\partial \theta} e^{i\omega t} \\ \zeta^\phi &= \frac{-r^l}{r^2 \sin^2 \theta} V(r) \frac{\partial Y_m^l}{\partial \phi} e^{i\omega t}, \end{aligned} \quad (16)$$

where  $W$  and  $V$  are amplitudes of the radial and transverse fluid perturbations. The equations governing these perturbation functions and the metric perturbations inside the star are given by [62,65]

$$\begin{aligned} \frac{dH_1}{dr} &= \frac{-1}{r} \left[ l+1 + \frac{2m}{r} e^{2\lambda} + 4\pi r^2 e^{2\lambda} (p - \epsilon) \right] H_1 \\ &+ \frac{1}{r} e^{2\lambda} [H + K + 16\pi(p + \epsilon)V], \end{aligned} \quad (17)$$

$$\begin{aligned} \frac{dK}{dr} &= \frac{l(l+1)}{2r} H_1 + \frac{1}{r} H - \left( \frac{l+1}{r} - \frac{d\Phi}{dr} \right) K \\ &+ \frac{8\pi}{r} (p + \epsilon) e^\lambda W, \end{aligned} \quad (18)$$

$$\begin{aligned} \frac{dW}{dr} &= r e^\lambda \left[ \frac{1}{\gamma p} e^{-\Phi} X - \frac{l(l+1)}{r^2} V - \frac{1}{2} H - K \right] \\ &- \frac{l+1}{r} W, \end{aligned} \quad (19)$$

$$\frac{dX}{dr} = \frac{-l}{r} X + (p + \epsilon) e^\Phi \left\{ \frac{1}{2} \left( \frac{d\Phi}{dr} - \frac{1}{r} \right) H \right.$$

$$\begin{aligned} &- \frac{1}{2} \left[ \omega^2 r e^{-2\Phi} + \frac{l(l+1)}{2r} \right] H_1 + \left( \frac{1}{2r} - \frac{3}{2} \frac{d\Phi}{dr} \right) K \\ &- \frac{1}{r} \left[ \omega^2 \frac{e^\lambda}{e^{2\Phi}} + 4\pi(p + \epsilon) e^\lambda - r^2 \frac{d}{dr} \left( \frac{e^{-\lambda}}{r^2} \frac{d\Phi}{dr} \right) \right] W \\ &\left. - \frac{l(l+1)}{r^2} \frac{d\Phi}{dr} V \right\}, \end{aligned} \quad (20)$$

$$\begin{aligned} &\left[ 1 - \frac{3m}{r} - \frac{l(l+1)}{2} - 4\pi r^2 p \right] H - 8\pi r^2 e^{-\Phi} X \\ &- \left[ 1 + \omega^2 r^2 e^{-2\Phi} - \frac{l(l+1)}{2} \right. \\ &\left. - (r - 3m - 4\pi r^3 p) \frac{d\Phi}{dr} \right] K \end{aligned} \quad (21)$$

$$\begin{aligned} &+ r^2 e^{-2\lambda} \left[ \omega^2 e^{-2\Phi} - \frac{l(l+1)}{2r} \frac{d\Phi}{dr} \right] H_1 = 0 \\ &e^{2\Phi} \left[ e^{-\phi} X + \frac{e^{-\lambda}}{r} \frac{dp}{dr} W + \frac{(p + \epsilon)}{2} H \right] \\ &- \omega^2 (p + \epsilon) V = 0, \end{aligned} \quad (22)$$

where  $X$  is introduced as [59,62]

$$X = \omega^2 (p + \epsilon) e^{-\Phi} V - \frac{We^{\Phi-\lambda}}{r} \frac{dp}{dr} - \frac{1}{2} (p + \epsilon) e^\Phi H, \quad (23)$$

and  $m = m(r)$  is the enclosed mass of the star and  $\gamma$  is the adiabatic index defined as

$$\gamma = \frac{(p + \epsilon)}{p} \left( \frac{\partial p}{\partial \epsilon} \right)_{\text{ad}}. \quad (24)$$

While solving the differential equations Eqs. (17)–(20) along with the algebraic Eqs. (21) and (22), we have to impose proper boundary conditions, i.e., the perturbation functions are finite throughout the interior of the star (particularly at the center, i.e., at  $r = 0$ ) and the perturbed pressure ( $\Delta p$ ) vanishes at the surface. Function values at the center of the star can be found using the Taylor series expansion method described in Appendix B of Ref. [59] (see also Appendix A of Ref. [62]). It is to be noted that the first term in right-hand side of Eq. (A15) in Ref. [62] misses a factor  $\epsilon$ ). The vanishing perturbed pressure at the stellar surface is equivalent to the condition  $X(R) = 0$  (as  $\Delta p = -r^l e^{-\Phi} X$ ). We followed the procedure described in LD [59] to find the unique solution for a given value of  $l$  and  $\omega$  satisfying all the boundary conditions inside the star.

### 2. Perturbations outside the star and complex eigenfrequencies

The perturbations outside the star are described by the Zerilli equation [66],

$$\frac{d^2 Z}{dr_*^2} + \omega^2 Z = V_Z Z, \quad (25)$$

where  $r_* = r + 2M \log(\frac{r}{2M} - 1)$  is the tortoise coordinate and  $V_Z$  is defined as [66]

$$V_Z = \frac{2(r - 2M)}{r^4(nr + 3M)^2} [n^2(n + 1)r^3 + 3n^2Mr^2 + 9nM^2r + 9M^3], \quad (26)$$

where  $n = \frac{1}{2}(l + 2)(l - 1)$ . Asymptotically the wave solution to (25) can be expressed as (27)

$$Z = A(\omega)Z_{\text{in}} + B(\omega)Z_{\text{out}},$$

$$Z_{\text{out}} = e^{-i\omega r^*} \sum_{j=0}^{j=\infty} \alpha_j r^{-j}, \quad Z_{\text{in}} = e^{i\omega r^*} \sum_{j=0}^{j=\infty} \bar{\alpha}_j r^{-j}. \quad (27)$$

Keeping terms up to  $j = 2$  one finds

$$\alpha_1 = -\frac{i}{\omega}(n + 1)\alpha_0, \quad (28)$$

$$\alpha_2 = \frac{-1}{2\omega^2} \left[ n(n + 1) - i3M\omega \left( 1 + \frac{2}{n} \right) \right] \alpha_0. \quad (29)$$

For initial boundary values of Zerilli functions, we use the method described in Refs. [60,62,67]. Setting  $m = M$  and perturbed fluid variables to 0 (i.e.,  $W = V = 0$ ) outside the star, connection between the metric functions (15) with Zerilli function  $[Z$  in Eq. (25)] can be written as

$$\begin{aligned} \begin{pmatrix} r^l K \\ r^{l+1} H_1 \end{pmatrix} &= Q \begin{pmatrix} Z \\ \frac{dZ}{dr_*} \end{pmatrix} \\ Q &= \begin{bmatrix} \frac{n(n+1)r^2 + 3nMr + 6M^2}{r^2(nr+3M)} & 1 \\ \frac{nr^2 - 3nMr - 3M^2}{(r-2M)(nr+3M)} & \frac{r^2}{r-2M} \end{bmatrix}. \end{aligned} \quad (30)$$

The initial boundary values of Zerilli functions are fixed using (30). Then the Zerilli equation (25) is integrated numerically to infinity and the complex coefficients  $A(\omega)$  and  $B(\omega)$  are obtained matching the analytic expressions for  $Z$  and  $\frac{dZ}{dr_*}$  with the numerically obtained value of  $Z$  and  $\frac{dZ}{dr_*}$ . The natural frequencies of an oscillating neutron star, which are not driven by incoming gravitational radiation, represent the quasinormal mode frequencies. Mathematically we have to find the complex roots of  $A(\omega) = 0$ , representing the complex eigenfrequencies of QNMs.

We tested our numerical technique by reproducing the quadrupole  $f$ -mode frequencies (complex) from Ref. [62] for polytropic stars (i.e., Table V and Fig. 5 of Ref. [62] wherein the method of continued fractions was used to find the complex eigenfrequencies).

## V. RESULTS

### A. Universal relations in NS asteroseismology

NS asteroseismology (inverse asteroseismology), the technique of inferring the NS parameters (internal composition) from QNM characteristics, was first introduced by Andersson and Kokkotas [37,38]. Theoretically, it was shown that the frequency of  $f$  mode varies linearly with density, whereas the damping time varies inversely with stellar compactness when scaled by  $M^3/R^4$ . Therefore empirical fit relations can

TABLE II. Asteroseismology relation coefficients for  $f$ -mode frequency from different works. The coefficients  $a_r$  and  $b_r$  are related to  $f$  by Eq. (31).

Reference	$a_r$ (kHz)	$b_r$ (kHz $\times$ km)
Andersson and Kokkotas [38]	0.22	47.51
Benhar and Ferrari [68]	0.79	33
D.Doneva <i>et al.</i> [25]	1.562	25.32
Pradhan and Chatterjee [40]	1.075	31.10
This work	0.535	36.20

be defined as follows:

$$f(\text{kHz}) = a_r + b_r \sqrt{\frac{M}{R^3}}, \quad (31)$$

$$\frac{R^4}{M^3 \tau_f} = a_i + b_i \frac{M}{R}. \quad (32)$$

where the constants  $a_r, b_r, a_i, b_i$  are extracted from the best fit to the data. The fits were subsequently improved by other works by including few selected realistic EoSs or those with exotic matter (hyperons and quarks) [68,69]. Further, NS rotation was considered by Doneva *et al.* [25], where empirical relations for frequency in nonrotating limits are also given. However, many of the selected EoSs considered in previous works are now incompatible with the  $\approx 2M_\odot$  maximum mass constraint or with the tidal deformability (radius) constraints from the event GW170817 and are hence ruled out.

It is worth noting that although the empirical relations obtained previously aim to be independent of the underlying EoS, all the proposed empirical fit relations are somewhat model dependent. The knowledge of mode frequencies and the NS masses (which is among the most precisely determined global variables) can therefore help to discriminate among the different EoSs, or to understand the behavior of high-density NS matter [70]. In other words, these empirical relations can be used not just to infer mass and radius but also to constrain the EoS stiffness and the presence of exotic matter [68]. Instead of choosing selected EoSs, we fit asteroseismology relations to cover the full range of uncertainties in nuclear and hypernuclear saturation parameters in the EoS subject to current astrophysical constraints. Empirical fit relations for frequency and damping time of  $f$ -modes from different works along with this work are tabulated in Table II and Table III, respectively. In this work we found  $a_r = 0.535 \pm 7.383 \times 10^{-4}$ ,  $b_r = 36.206 \pm 0.019$ ,  $a_i = (7.99 \pm 0.002) \times 10^{-2}$ , and  $b_i = -0.245 \pm 1.005 \times 10^{-4}$ . One may compare the fit results

TABLE III. Asteroseismology relation coefficients for  $f$ -mode damping time from different works. The coefficients  $a_i$  and  $b_i$  are related to  $\tau_f$  by Eq. (32).

Reference	$a_i$	$b_i$
Andersson and Kokkotas [38]	0.086	-0.267
Benhar and Ferrari [68]	0.087	-0.271
This work	0.080	-0.245

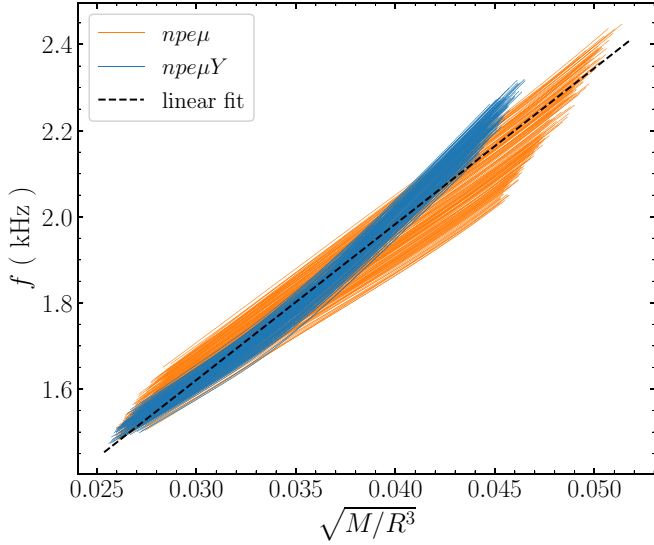


FIG. 3. The  $f$ -mode frequencies as a function of square root of the mean density. Models with only nuclear (nucleon and hyperon) matter are shown in orange (blue) lines and the empirical linear fit relation (31) by black dashed line.

within Cowling approximation [40] and full GR calculations (this work) for  $a_r$  and  $b_r$  from Table II. The dependence of frequency (scaled damping time) with density (compactness) is displayed in Fig. 3 (Fig. 4), along with empirical fit relation Eq. (31) [Eq. (32)]. Please note that the coefficients given in Ref. [38] were incorrect due to a normalization error in the calculation [71]. These values have now been updated in Table II.

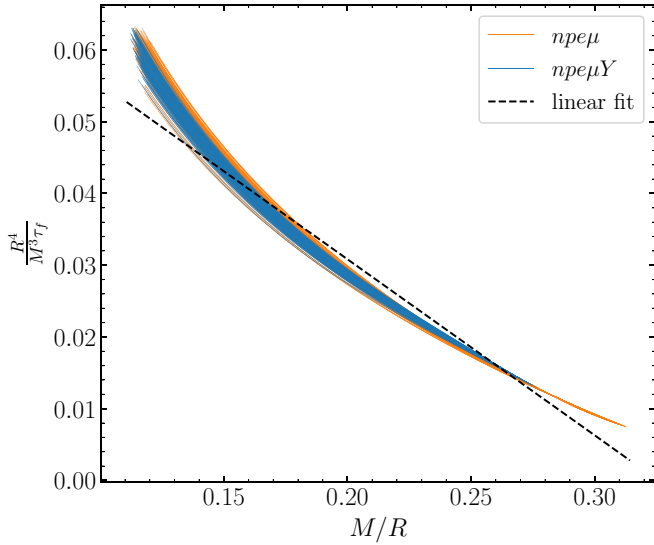


FIG. 4. Scaled damping time of  $f$  mode as a function of stellar compactness  $M/R$ . Models with only nuclear (nucleon and hyperon) matter are shown in orange (blue) lines and the empirical linear fit relation (32) by black dashed line.

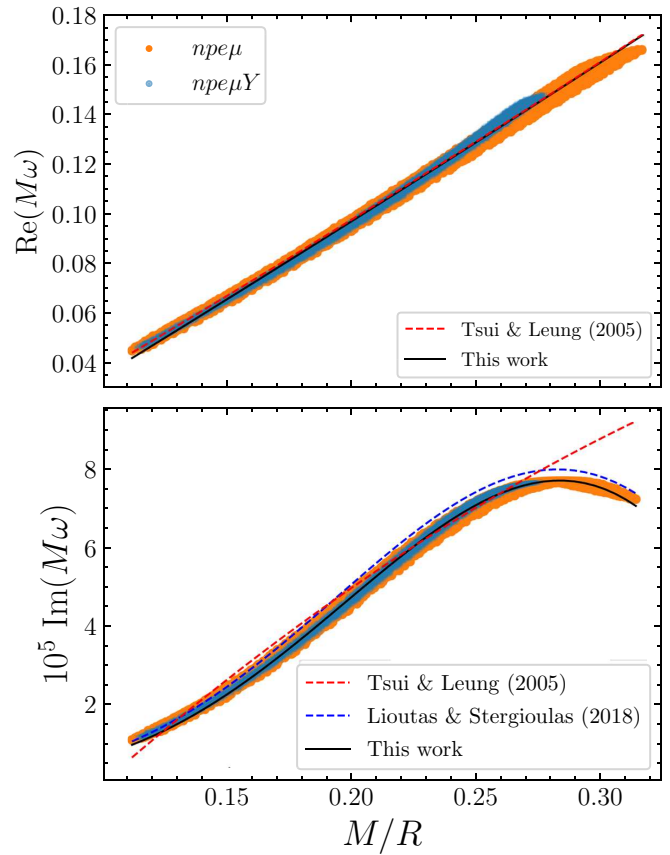


FIG. 5. Dependence of QNM frequency after scaling with NS mass as a function of stellar compactness. Scattered orange (blue) points correspond to models with  $npe\mu$  ( $npe\mu Y$ ) matter. The region spanned by hyperonic stars comes within the region spanned by the nucleonic models. The upper panel shows the universality for real part of  $M\omega$ , while the lower panel shows the universality of mass scaled by damping time [ $\frac{M}{\tau_f}$  or  $\text{Im}(M\omega)$ ].

Contrary to empirical fit relations (31) and (32) which are model dependent, there are other proposed universal relations (UR), which are fairly independent of underlying composition hence, more useful for extracting the NS parameter from QNM observables. It was shown when the mode characteristics are scaled with NS mass or radius they show correlations with the stellar compactness [38] and the relations can be expressed in a universal way. In our previous work [40] we found the universality between scaled frequency with stellar compactness holds when  $\omega$  scaled with NS mass but deviates from universality when scaled by radius. Tsui and Leung [72] explicitly demonstrated that the scaled polar QNM frequencies of realistic neutron stars are approximately given by a universal function of the compactness and improved the linear UR to quadratic fit, as given in Eq. (33). We note in Fig. 5 that a similar quadratic fit for  $\text{Im}(M\omega)$  given in Ref. [72] deviates from universality at large compactness, whereas Eq. (34) proposed by Lioutas and Stergioulas [73] provides a better fit. We display the dependence of scaled complex QNM frequency (scaled with NS mass),  $M\omega$  as a function of compactness along with the URs from this and past works in Fig. 5. Fit

TABLE IV. Fit parameters for the URs (33) and (34) obtained in this work.

	$\text{Re}(M\omega)$	$\text{Im}(M\omega)$
$a_0$	$0.079 \pm 0.002$	$b_0$ $(9.836 \pm 0.003) \times 10^{-2}$
$a_1$	$0.599 \pm 0.001$	$b_1$ $(-4.448 \pm 0.002) \times 10^{-1}$
$a_2$	$-0.026 \pm 8 \times 10^{-5}$	$b_2$ $(4.915 \pm 0.004) \times 10^{-1}$

parameters corresponding to URs (33) and (34) found in this work are tabulated in Table IV,

$$\text{Re}(M\omega) = a_0 \left( \frac{M}{R} \right)^2 + a_1 \frac{M}{R} + a_2, \quad (33)$$

$$\text{Im}(M\omega) = b_0 \left( \frac{M}{R} \right)^4 + b_1 \left( \frac{M}{R} \right)^5 + b_2 \left( \frac{M}{R} \right)^6. \quad (34)$$

In a binary NS system, during the inspiral phase, NSs deform each other by exerting strong gravitational forces and the deformation depends on the underlying EoS. The analysis of the tidal deformability from the event GW1701817 plays a crucial role in constraining NS EoS. From our current understanding of merger simulations, the mass scaled peak frequency ( $f_{\text{peak}}$ ) of the post merger phase shows universality with tidal deformability or compactness [74–77]. It was pointed out recently by Chakravarti and Andersson [78] that the universality between  $f_{\text{peak}}$  and tidal deformability can be explained by adding the rotational and thermal corrections to the existing universal relation between mode frequency and tidal deformability of cold nonrotating neutron stars and the total mass scaled  $f_{\text{peak}}$  frequency can be expressed as a scaling factor times the mass scaled  $f$ -mode frequency. Also during the inspiral phase the  $f$  modes are most likely to be excited and observation of  $f$ -mode frequency along with tidal deformability can be used to probe the NS interior. Analyzing the event GW170817 along with the universality behavior of frequency and tidal deformability should allow one to put a lower bound on the  $f$ -mode frequencies for NSs within the mass range of the two binary components of GW170817 [33].

It was argued that the  $f$ -mode frequencies can be detected very accurately with improved sensitivity of GW detectors, whereas damping time may not be detected with such good accuracy [79]; in this case the universal relations can be helpful in constraining the damping time. The detection of  $f$ -mode characteristics [70] or  $f_{\text{peak}}$  [77] along with tidal deformability can also be used to verify the presence of quarks in the interior of NS. We provide the UR between  $f$ -mode characteristics and tidal deformability as suggested in Refs. [31,80]. We tabulate the complex  $\alpha_j$  from (35) found in this work in Table V

TABLE V. Values of the fit parameters  $\alpha_j$  found in this work for the given equation (35).

$\alpha_0$	$\alpha_1$	$\alpha_2$	$\alpha_3$	$\alpha_4$	$\alpha_5$
$1.814 \times 10^{-1} + i3.362 \times 10^{-5}$	$-5.824 \times 10^{-3} + i3.993 \times 10^{-5}$	$-4.725 \times 10^{-3} - i1.0215 \times 10^{-5}$	$6.337 \times 10^{-4} + i1.270 \times 10^{-7}$	$-2.871 \times 10^{-5} + i1.230 \times 10^{-7}$	$3.150 \times 10^{-7} - i7.817 \times 10^{-9}$

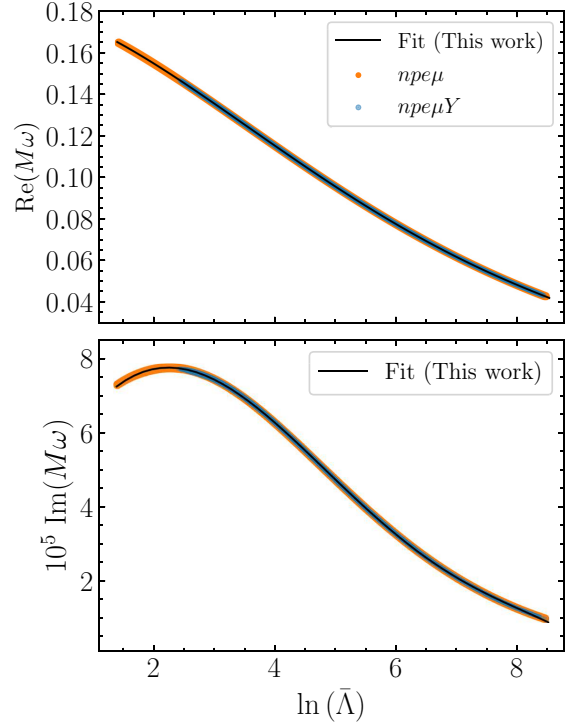


FIG. 6. Dependence of QNM frequency after scaling with NS mass as a function of dimensionless tidal deformability. Scattered orange (blue) points correspond to model with  $npem$  ( $npemY$ ) matter. The region spanned by hyperonic stars comes within the region spanned by the nucleonic models. The upper panel shows the universality for real part of  $M\omega$ , while the lower panel shows the universality of mass scaled by damping time [ $\frac{M}{\tau_f}$  or  $\text{Im}(M\omega)$ ].

and display in Fig. 6,

$$M\omega = \sum_j \alpha_j (\ln \bar{\Lambda})^j. \quad (35)$$

We also found that there exists a universal relation between QNM characteristics (i.e., frequency and damping time) when they are scaled by NS mass. The universal relation between mass scaled angular frequency [ $\text{Re}(M\omega)$ ] and mass scaled damping time [ $\text{Im}(M\omega)$  or  $M/\tau_f$ ] can be described by the following relation:

$$\text{Im}(M\omega) = \sum_j \gamma_j [\text{Re}(M\omega)]^j. \quad (36)$$

We tabulate the fit parameters of Eq. (36) in Table VI.

Even in a binary NS system, there exists universality between mode characteristics and tidal deformability in the inspiral phase [31,70] and between  $f_{\text{peak}}$  and tidal deformability [77]. With future detections of BNS merger events the

TABLE VI. Values of the fit parameters  $\gamma_j$  found in this work for the given equation (36).

$\gamma_0$	$\gamma_1$	$\gamma_2$	$\gamma_3$	$\gamma_4$	$\gamma_5$
$6.002 \times 10^{-6}$	$-4.053 \times 10^{-4}$	$1.339 \times 10^{-2}$	$-6.577 \times 10^{-2}$	$2.620 \times 10^{-1}$	-1.072

constraint on the tidal deformability will improve, and these in turn can then be used to constrain the mode characteristics. Our result for the lower bound on the mode frequency is in good agreement with the limit obtained from observations of GW170817 [33]. In order to test this hypothesis, we display the dependence of  $f$ -mode frequency as a function of tidal deformability for canonical NSs in Fig. 7. Looking at the points corresponding to the maximum limit of the tidal deformability of a  $1.4M_\odot$  in Fig. 7, one can conclude that for a  $1.4M_\odot$  the lower bound on mode frequency will be around 1.60 kHz. Similarly, we found the upper bound on  $\tau_f$  for a  $1.4M_\odot$  NS to be 0.28 s.

## B. Correlation studies

The uncertainty in the EoS and hence in mass-radius relations corresponding to uncertainty associated with nuclear and hypernuclear saturation data are discussed in Sec. II B. Having tested our numerical scheme for complex  $f$ -mode frequencies, and obtained scaling relations with neutron star global parameters, we now extend our investigation to study the effect of microscopic (saturation) parameters on the  $f$ -mode observables ( $f$  and  $\tau_f$ ).

### 1. Nucleonic matter

We first consider only nucleonic EoSs to find the effect of nuclear saturation data on NS observables and then

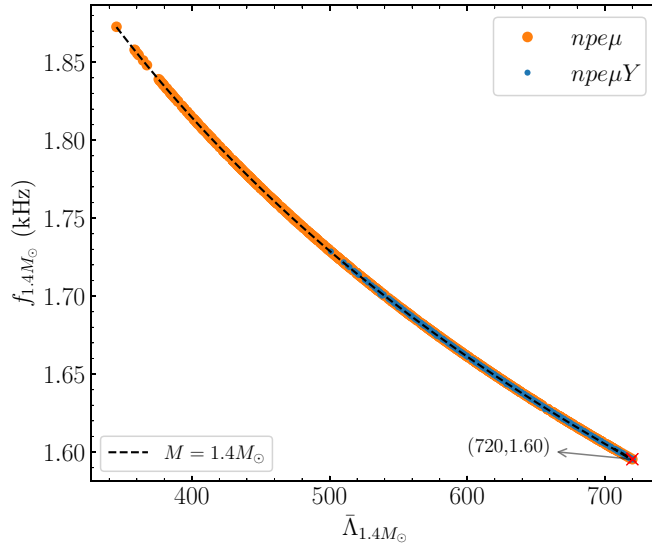


FIG. 7. Universality between  $f$ -mode frequencies and tidal deformability ( $\bar{\Lambda}$ ) of a canonical  $1.4M_\odot$  NS. Scattered orange (blue) points correspond to models with  $npe\mu$  ( $npe\mu Y$ ) matter. The black dashed line is obtained using the UR (35). The red crossed point is corresponding to the maximum limit for  $(\bar{\Lambda})_{1.4M_\odot}$ .

extend to involve hyperons. For better understanding, we obtained the Pearson's correlation coefficients ( $R_{X_1 X_2}$ ) among the saturation parameters, NS observables such as radius and tidal deformability and QNM characteristic for canonical  $1.4M_\odot$ , and massive  $2M_\odot$  NSs. Pearson's linear correlation coefficient ( $R_{X_1 X_2}$ ) between two random variables  $X$  and  $Y$  can be defined as [81]

$$R_{X_1 X_2} = \frac{\text{Cov}(X_1, X_2)}{S(X_1)S(X_2)}, \quad (37)$$

where  $\text{Cov}(X_1, X_2)$  is the covariance and  $S(X_i)$  denotes standard deviation of variable  $X_i$ . We present the correlation matrix in Fig. 8. From Fig. 8 the following conclusions can be drawn:

- NS observables show strong correlation among themselves as well as with the QNM characteristics. As expected from (13)  $\bar{\Lambda}$  shows a strong correlation with  $R$  (0.97 for  $1.4M_\odot$  and 0.98 for  $2M_\odot$ ). Frequency and damping time also show a strong correlation among themselves.
- We find strong correlations between  $f$ -mode frequency and radius which can be explained by looking at (31) given in Sec. V A, similarly the high correlation between damping time and radius can be explained by (32) from Sec. V A.
- Among the saturation parameters  $m^*$  shows strong correlations with radius and tidal deformability (0.85

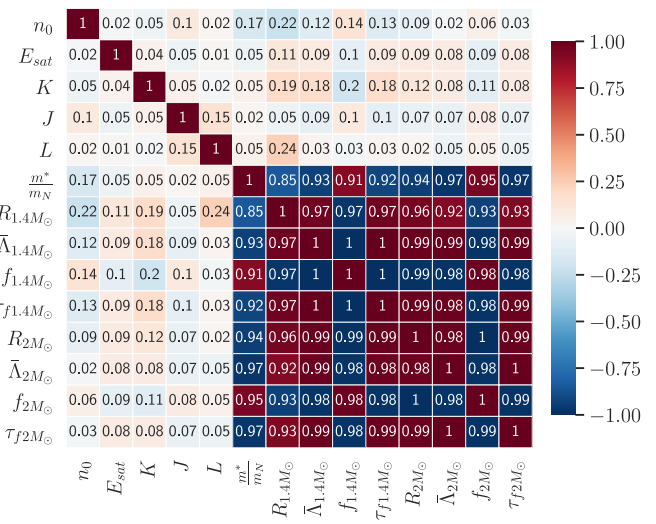


FIG. 8. Correlation matrix for nuclear saturation parameters, NS observables, and QNM characteristics considering models with  $npe\mu$  matter after applying astrophysical constraint ( $M_{\text{max}} \geq 2M_\odot$  and  $\bar{\Lambda}_{1.4M_\odot} \leq 720$ ). In the color bar the correlation changes from positive to negative going from red to blue in color. However, the absolute value of correlations are written in the correlation matrix.

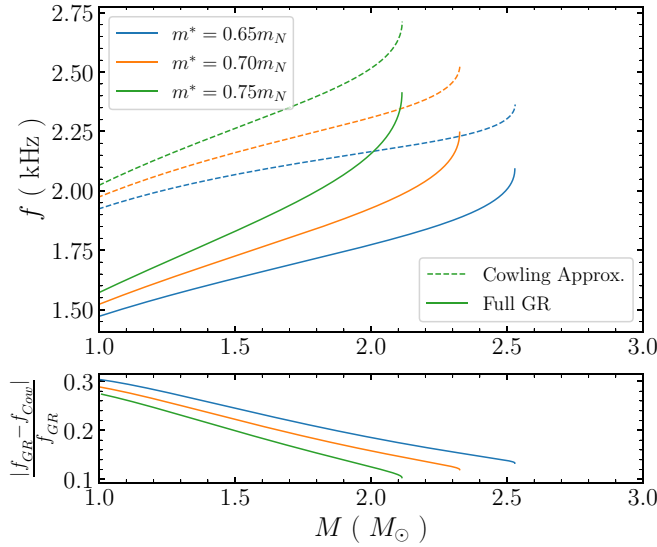


FIG. 9. The  $f$ -mode frequencies of stable NS configurations as a function of stellar mass (upper panel) with  $npe\mu$  matter for different nuclear effective mass ( $m^*$  at saturation). For comparison, results obtained using Cowling approximation (dashed lines) and obtained in full GR (solid lines) are shown. Lower panel shows relative error for  $f$ -mode frequencies obtained using two different methods. While varying  $m^*$  other parameters are fixed at,  $n_0 = 0.150 \text{ fm}^{-3}$ ,  $E_{\text{sat}} = -16.0 \text{ MeV}$ ,  $J = 32 \text{ MeV}$ ,  $L = 60 \text{ MeV}$ , and  $K = 240 \text{ MeV}$ .

with  $R$  and 0.93 with  $\bar{\Lambda}$  for  $1.4M_\odot$ ) which is expected as  $m^*$  is the dominant parameter controlling the stiffness of EoS and hence the radius.

(iv) Strong correlations exist between mode characteristics ( $f$  and  $\tau_f$ ) and nucleon effective mass ( $m^*$ ) for  $1.4M_\odot$  (0.91 with  $f$  and 0.92 with  $\tau_f$ ) as well as for  $2M_\odot$  (0.95 with  $f$  and 0.97 with  $\tau_f$ ). This leads us to conclude that the nucleon effective mass has the most dominant effect on the QNM characteristics compared to other nuclear saturation parameters.

We display the dependence of frequency and damping time as a function of stellar mass for variation of  $m^*$  in Fig. 9 and Fig. 10, respectively. Extension of our previous calculations from Cowling to involve linearized gravity provides us an opportunity to compare the  $f$ -mode frequencies from the two different methods. We display a comparison of frequency obtained by two different methods with variation of nucleon effective mass  $m^*$  in Fig. 9. We find Cowling approximation can include error of 10–30% in the quadrupole  $f$ -mode frequencies and the error decreases with increasing mass. The obtained trend of decreasing error with increasing mass is in good agreement with the previous result from Ref. [56]. A possible explanation for this trend was discussed in Ref. [82], given that the  $f$ -mode eigenfunction is peaked near the surface, increasing mass (or compactness for the given mass range and models considered) can make the metric perturbations less relevant for  $f$ -mode eigenfunction resulting in a smaller error compared to the frequency obtained within the relativistic Cowling approximation.

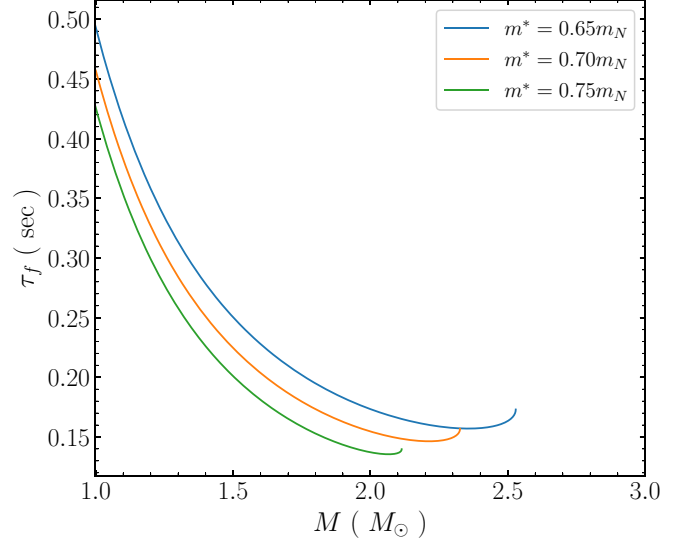


FIG. 10. The  $f$ -mode damping time as a function of stellar mass with  $npe\mu$  matter for different  $m^*$ . While varying  $m^*$  other parameters are fixed to  $n_0 = 0.150 \text{ fm}^{-3}$ ,  $E_{\text{sat}} = -16.0 \text{ MeV}$ ,  $J = 32 \text{ MeV}$ ,  $L = 60 \text{ MeV}$ , and  $K = 240 \text{ MeV}$ .

## 2. Inclusion of hyperons

We extend our investigation by including presence of hyperons in the NS core and present the correlation matrix in Fig. 11 in a similar fashion as given for nucleonic models. Looking at Fig. 11 one can conclude the following:

(i) NS observables show strong correlations among themselves as well as with the QNM characteristics.

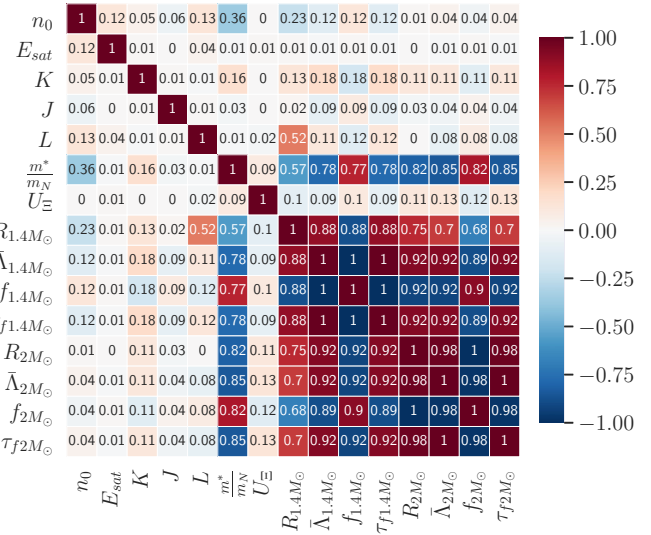


FIG. 11. Correlation matrix for nuclear saturation parameters, NS observables, and QNM characteristics considering models with  $npe\mu Y$  matter after applying astrophysical constraints ( $M_{\text{max}} \geq 2M_\odot$  and  $\bar{\Lambda}_{1.4M_\odot} \leq 720$ ). In the color bar the correlation changes from positive to negative going from red to blue in color. However, the absolute value of correlations are written in the correlation matrix.

- (ii) Interestingly the correlation between  $L$  and radius of  $1.4M_{\odot}$  star increases when compared to the nucleonic case (from 0.24 to 0.52) while the correlation between  $m^*$  and  $R_{1.4M_{\odot}}$  decreases from 0.85 to 0.57 compared to the nucleonic case.
- (iii) However, when it comes to QNM characteristics, they show strong correlations with  $m^*$  for a  $1.4M_{\odot}$  star as well as for a  $2M_{\odot}$  star. It is worth noting that the correlations among  $m^*$  and NS observables have decreased compared to the models with only nucleonic EoSs.

In light of these inferences from the correlation plot Fig. 11, one can conclude that the  $m^*$  has the most dominant effect on the QNM characteristics compared to other nuclear and hypernuclear saturation parameters, even in the presence of hyperons.

## VI. DISCUSSIONS

### A. Summary of this work

We revisit the NS asteroseismology problem in this work, considering realistic EoSs in the RMF framework and current astrophysical constraints. In a recent publication [40], we studied the effect of the influence of the uncertainties in the underlying nuclear and hypernuclear physics on *f*-mode frequencies within the relativistic Cowling approximation. Here we extend this work to study the effect of uncertainties in the underlying nuclear and hypernuclear physics on complex *f*-mode characteristics (frequency and damping time) of nonrotating perturbed NSs by solving the perturbation equations based on complete linearized equations in general relativity. We provide the asteroseismology relations by considering EoSs with the nuclear and hypernuclear matter in the NS core.

Previous works on NS asteroseismology or inverse asteroseismology involved selected realistic or polytropic EoSs. Many of the chosen EoSs have now been rendered incompatible with large NS mass observations or the tidal deformability constraint from merger event GW170817. Hence the empirical relations from past works need to be modified. There are a few efforts to investigate the effect on *f* modes of the inclusion of exotic forms of matter (hyperon or quark matter) [54,55,68,69,83–85] or to improve the asteroseismology relations with current astrophysical constraints [80,86–88]. However, the works are either limited to selective EoSs or used Cowling approximation to find the mode characteristics.

As mentioned, the extension of our previous work [40] (where relativistic Cowling approximation was used to find the mode frequency), by involving complete linearized equations of general relativity, allows us to compare the mode frequencies obtained within the two different methods. For the models considered, frequencies obtained using relativistic Cowling approximation can include an error up to 30% compared to those obtained in full general relativity. Solving the NS oscillation in full general relativity enables us to investigate the effect of uncertainties in the underlying nuclear and hypernuclear physics on both frequency and damping time of the *f* mode. The dependence of mode frequencies on the stellar mass remains qualitatively similar (increasing)

to results obtained using relativistic Cowling approximation irrespective of the composition of the NS interior. The *f*-mode damping time shows an inverse relation with NS mass for both nuclear and hypernuclear matter EoSs. Considering NS masses starting from  $1M_{\odot}$  and up to the possible maximum stable NS mass configuration of each model along with current astrophysical constraints, the frequency and damping time of quadrupole *f*-mode oscillations are found to be in the range of 1.47–2.45 kHz and 0.13–0.51 s, respectively. In this work, we also obtained the UR involving tidal deformability and mass scaled *f*-mode characteristics. We tested the hypotheses of universality between tidal deformability for a canonical  $1.4M_{\odot}$  NS. Using the upper bound of tidal deformability, we found the lower bound on the  $f_{1.4M_{\odot}}$  to be 1.6 kHz, which is in agreement with the result obtained with Bayesian estimation from Pratten *et al.* [33]. We also found that, using the upper bound of the tidal deformability coming from the event GW170817 for a  $1.4M_{\odot}$  (i.e.,  $\bar{\Lambda} \leq 720$ ), the damping time of a  $1.4M_{\odot}$  has an upper limit of 0.28 s. From Fig. 7, it is evident that frequencies above 1.7 kHz are difficult to describe with hyperonic EoSs in our model.

We found that while considering nucleonic EoSs and imposing current astrophysical constraints, among all the nuclear saturation parameters, the nuclear effective mass  $m^*$  has the most dominant effect on *f*-mode characteristics. We explored correlations among saturation parameters, NS observables (radius and tidal deformability), and *f*-mode characteristics for a canonical  $1.4M_{\odot}$  and a massive  $2M_{\odot}$ . NS observables show strong correlations among themselves as well as with *f*-mode characteristics. The strong correlations of  $m^*$  with NS observables ( $R_{1.4M_{\odot}}, \bar{\Lambda}_{1.4M_{\odot}}$ ) and *f*-mode characteristics ( $f_{1.4M_{\odot}}, \tau_{f1.4M_{\odot}}$ ) for NS with  $1.4M_{\odot}$  remain so even for  $2M_{\odot}$ .

We further investigate the effect of uncertainties in nuclear and hypernuclear saturation parameters on the *f*-mode characteristics by considering the presence of hyperons on the NS interior along with the imposition of current astrophysical constraints. We checked that even in the presence of hyperons, the nuclear effective mass ( $m^*$ ) still has the dominant effect on the *f*-mode characteristics. The hypernuclear parameter  $U_{\Xi}$  was found to have a minor effect on *f*-mode characteristics. We also provide correlations among the nuclear saturation parameters, hypernuclear parameters as well as with the NS observables (radius and tidal deformability) and *f*-mode characteristics for a  $1.4M_{\odot}$  and a massive  $2M_{\odot}$  for hyperonic stars. Similarly to nuclear-matter models, NS observables show strong correlations among themselves and also with *f*-mode characteristics. Considering the presence of hyperons in the NS core and imposing the maximum mass limit of  $2M_{\odot}$  and  $\bar{\Lambda}_{1.4M_{\odot}} \leq 720$ , the correlation between slope of symmetry energy at saturation ( $L$ ) and  $R_{1.4M_{\odot}}$  increases in comparison with nucleonic models whereas the correlation between  $m^*$  and  $R_{1.4M_{\odot}}$  decreases.

In our analysis, we provide URs in asteroseismology considering the entire parameter range of uncertainties within the framework of the RMF model compatible with state-of-the-art nuclear and hypernuclear physics subject to current astrophysical constraints. These empirical relations involving *f*-mode frequency and average density or appropriately scaled damping time and stellar compactness differ in their fit

parameters compared to those proposed previously in the literature [37,38,68]. Also in full general relativity, we found the empirical fits between frequency and density to be dependent on the choice of EoSs considered. We then tested the hypotheses of universality between stellar compactness and  $f$ -mode characteristics scaled with stellar mass. We provide a quadratic universal relation among mass scaled angular frequency and stellar compactness [ $\text{Re}(M\omega)=F_1(M/R)$ ] and a universal relation for mass scaled damping time and stellar compactness [i.e.,  $\text{Im}(M\omega)=\text{Im}(M/\tau_f)=F_2(M/R)$ ]. When the angular frequencies and damping times are scaled appropriately with NS mass, the universality between  $f$ -mode frequency and damping time can be described by the proposed UR.

### B. Future prospects

During the inspiral phase of a binary NS merger, when the tidal field reaches resonance with the NS internal oscillation modes, particular new features are created in the GW waveform that, if detected, can provide information on the QNMs. Among these modes, the  $f$  mode is the most important one. Hence studying the effect of dynamical tides can be used to analyze the influence of QNM modes in the merger waveform [33,89]. In merger events, tidal deformability is another important observable parameter. Future detection will put tight constraints on tidal deformability; hence universal relations involving  $f$ -mode characteristics and tidal deformability are useful for analyzing the mode characteristics.

To understand the  $f$  modes thoroughly, other complicating effects such as rotation [25,30,63], magnetic fields, the effect of superfluidity [90], and the presence of deconfined quark core should be taken into account. Superfluidity will play a role in the case of cold NSs, whereas rotation will play a crucial role in the hot and differentially rotating merger remnant. It has been shown that for stars with deconfined quarks in NS interior, the  $f$ -mode vs tidal deformability relation deviates from the universality in isolated NSs [70] as well as in merger remnants [77].

### C. Detectability

We conclude by making some remarks on the detectability of the  $f$ -mode of hyperonic stars. As the  $f$ -mode amplitude peaks near the star's surface, it may be excited strongly by glitching behavior in an isolated star or by tidal forces due to a companion during the late inspiral in a merger. In the former case, one would expect a GW burst in the detector, while in the latter case, the  $f$  mode would draw energy from the orbit, affecting the phase of the gravitational waveform. The study by Pratten *et al.* [33] placed a lower bound on the quadrupolar  $f_2$ -mode in the region of 1400 Hz, including the mode excitation directly as a parameter in the analysis of data from GW170817. Here we will consider isolated hyperonic stars that emit a burst of GW due to the  $f$  mode and estimate the peak gravitational wave strain and associated energy required for detection in aLIGO and third generation detectors. Utilizing the methodology in Ref. [91], wherein the burst waveform is modelled as an exponentially damped oscillation with frequency  $\nu_f$  and damping time  $\tau_f$ , we find the peak

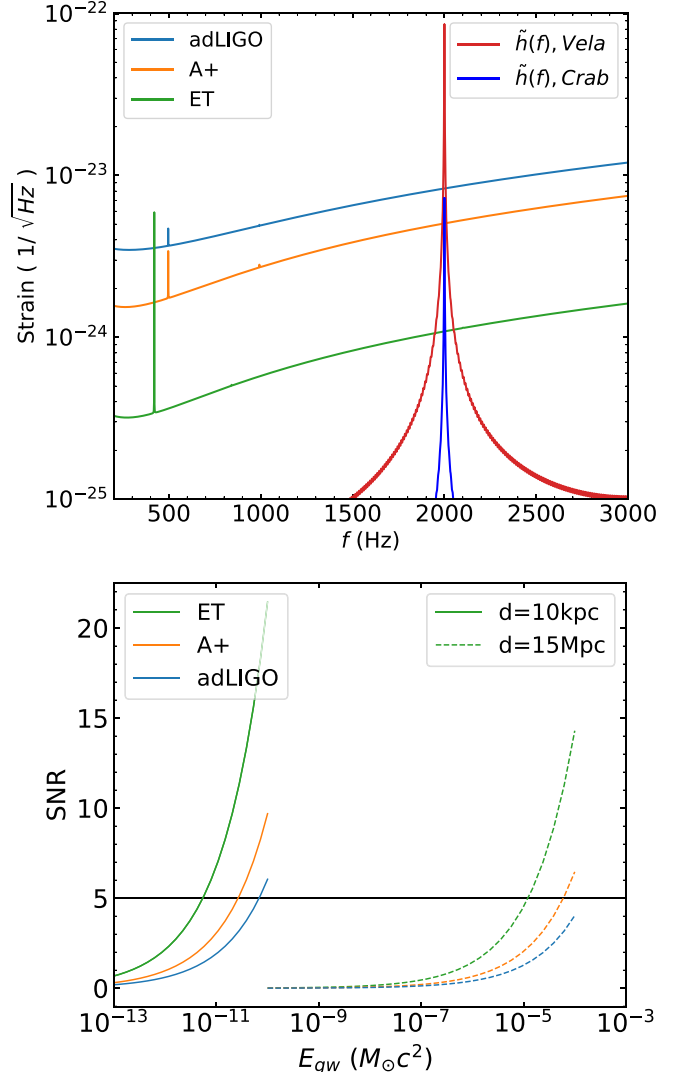


FIG. 12. Top panel: Gravitational wave strain corresponding to a maximum glitch energy observed in Vela pulsar (Crab pulsar) with distance to be 290 pc (2 kpc) are shown along with the sensitivity bands of different configurations. The waveforms are generated using the GW inference package Bilby [92]. Lower panel: Signal-to-noise ratio (SNR) for a source with  $f$ -mode frequency 1.70 kHz and damping time 0.25 s at different detector configurations as a function of  $E_{\text{GW}}$  for sources to be at 10 kpc (solid lines) or at 15 Mpc (dashed lines).

strain

$$h_0 = 1.46 \times 10^{-13} \sqrt{\frac{E_{\text{GW}}}{M_{\odot}c^2}} \sqrt{\frac{1 \text{ s}}{\tau_f} \frac{1 \text{ kpc}}{d}} \left( \frac{1 \text{ kHz}}{\nu_f} \right). \quad (38)$$

Choosing a canonical NS mass of  $1.4M_{\odot}$  at a distance of 10 kpc, an  $f$ -mode frequency of 1.70 kHz with a damping time of 0.25 s, and assuming that  $E_{\text{GW}}$  is of the order of a glitch in the Vela pulsar and highly efficient in producing GW, Figure 12 (top panel) shows the resulting frequency domain waveform  $\tilde{h}(f)$  against the sensitivity curve of advanced LIGO (aLIGO) [93], A+ [94] and the Einstein Telescope

(ET) [95,96] and the  $E_{\text{GW}}$  (bottom panel) required for the typical signal-to-noise ratio ( $\text{SNR} \approx 5$ ) for detection in these instruments. For sources at 10 kpc for  $\text{SNR} \geq 5$ , the energy  $E_{\text{GW}}$  should be greater than  $5.75 \times 10^{-12} M_{\odot} c^2$ ,  $2.88 \times 10^{-11} M_{\odot} c^2$ , and  $6.88 \times 10^{-11}$  for ET, A+ and adLIGO configuration, respectively. For sources at 15 Mpc for  $\text{SNR} \geq 5$  in A+ and ET configuration  $E_{\text{GW}}$  should be greater than  $6.55 \times 10^{-5} M_{\odot} c^2$  and  $1.3 \times 10^{-5} M_{\odot} c^2$ , respectively. As  $E_{\text{GW}}$  is a parameter in the waveform, depending on the distance, GWs induced from (i) NS glitches, (ii) a supernova explosion, or (iii) a prominent phase transition, leading to a mini collapse in NS are possible sources that could be detectable. These might be considered optimistic estimates, given that most glitches are weaker than in Vela pulsar and might not couple that strongly to GW. In addition, individual sources

may have considerable uncertainty in either the distance or radius parameters. The statistical approach followed in Ref. [91] uses the BSk24 EOS (no hyperons or exotic matter) to model ordinary neutron stars satisfying current observational constraints and suggests that third generation detectors like ET and Cosmic Explorer would offer the best chance to detect the transient bursts from *f* modes.

## ACKNOWLEDGMENTS

P.J. is supported by the US National Science Foundation Grant No. PHY-1913693. B.-K.P. and D.C. acknowledge usage of the IUCAA HPC computing facility for the numerical calculations. B.-K.P. is thankful to Suprovo Ghosh, Dhruv Pathak, Swarnim Shirke, and Tathagata Ghosh for their useful discussions during this work.

---

[1] I. Vidaña, Short introduction to the physics of neutron stars, *EPJ Web Conf.* **227**, 01018 (2020).

[2] J. M. Lattimer and M. Prakash, The physics of neutron stars, *Science* **304**, 536 (2004).

[3] J. M. Lattimer and M. Prakash, Neutron star observations: Prognosis for equation of state constraints, *Phys. Rep.* **442**, 109 (2007).

[4] D. Chatterjee and I. Vidaña, Do hyperons exist in the interior of neutron stars? *Eur. Phys. J. A* **52**, 29 (2016).

[5] W.-C. Chen and J. Piekarewicz, Building relativistic mean field models for finite nuclei and neutron stars, *Phys. Rev. C* **90**, 044305 (2014).

[6] N. Hornick, L. Tolos, A. Zacchi, J.-E. Christian, and J. Schaffner-Bielich, Relativistic parameterizations of neutron matter and implications for neutron stars, *Phys. Rev. C* **98**, 065804 (2018).

[7] P. Demorest, T. Pennucci, S. Ransom, M. Roberts, and J. Hessels, Shapiro delay measurement of a two solar mass neutron star, *Nature (Lond.)* **467**, 1081 (2010).

[8] J. Antoniadis *et al.*, A massive pulsar in a compact relativistic binary, *Science* **340**, 1233232 (2013).

[9] H. T. Cromartie, E. Fonseca, S. M. Ransom, P. B. Demorest, Z. Arzoumanian, H. Blumer, P. R. Brook, M. E. DeCesar, T. Dolch, J. A. Ellis *et al.*, Relativistic shapiro delay measurements of an extremely massive millisecond pulsar, *Nat. Astron.* **4**, 72 (2020).

[10] E. Fonseca, T. T. Pennucci, J. A. Ellis, I. H. Stairs, D. J. Nice, S. M. Ransom, P. B. Demorest, Z. Arzoumanian, K. Crowter, T. Dolch *et al.*, The nanograv nine-year data set: Mass and geometric measurements of binary millisecond pulsars, *Astrophys. J.* **832**, 167 (2016).

[11] T. E. Riley, A. L. Watts, P. S. Ray, S. Bogdanov, S. Guillot, S. M. Morsink, A. V. Bilous, Z. Arzoumanian, D. Choudhury, J. S. Deneva, K. C. Gendreau, A. K. Harding, W. C. G. Ho, J. M. Lattimer, M. Loewenstein, R. M. Ludlam, C. B. Markwardt, T. Okajima, C. Prescod-Weinstein, R. A. Remillard *et al.*, A NICER view of the massive pulsar PSR j0740+6620 informed by radio timing and XMM-newton spectroscopy, *Astrophys. J. Lett.* **918**, L27 (2021).

[12] Z. Arzoumanian, K. C. Gendreau, C. L. Baker, T. Cazeau *et al.*, The neutron star interior composition explorer (NICER): Mission definition, in *Space Telescopes and Instrumentation 2014: Ultraviolet to Gamma Ray*, edited by T. Takahashi, J.-W. A. den Herder, and M. Bautz (SPIE, Bellingham, WA, 2014), Vol. 9144, pp. 579–587.

[13] M. C. Miller, F. K. Lamb, A. J. Dittmann, S. Bogdanov, Z. Arzoumanian, K. C. Gendreau, S. Guillot, A. K. Harding, W. C. G. Ho, J. M. Lattimer *et al.*, Psr j0030+0451 mass and radius from nicer data and implications for the properties of neutron star matter, *Astrophys. J.* **887**, L24 (2019).

[14] T. E. Riley, A. L. Watts, S. Bogdanov, P. S. Ray, R. M. Ludlam, S. Guillot, Z. Arzoumanian, C. L. Baker, A. V. Bilous, D. Chakrabarty *et al.*, A nicer view of psr j0030+0451: Millisecond pulsar parameter estimation, *Astrophys. J.* **887**, L21 (2019).

[15] E. E. Flanagan and T. Hinderer, Constraining neutron-star tidal love numbers with gravitational-wave detectors, *Phys. Rev. D* **77**, 021502(R) (2008).

[16] B. Abbott, R. Abbott, T. Abbott, F. Acernese, K. Ackley, C. Adams, T. Adams, P. Addesso, R. Adhikari, V. Adya *et al.*, Gw170817: Observation of Gravitational Waves from a Binary Neutron Star Inspiral, *Phys. Rev. Lett.* **119**, 161101 (2017).

[17] B. Abbott, R. Abbott, T. Abbott, F. Acernese, K. Ackley, C. Adams, T. Adams, P. Addesso, R. Adhikari, V. Adya *et al.*, Gw170817: Measurements of Neutron Star Radii and Equation of State, *Phys. Rev. Lett.* **121**, 161101 (2018).

[18] B. Abbott, R. Abbott, T. Abbott, F. Acernese, K. Ackley, C. Adams, T. Adams, P. Addesso, R. Adhikari, V. Adya *et al.*, Properties of the Binary Neutron Star Merger Gw170817, *Phys. Rev. X* **9**, 011001 (2019).

[19] B. P. Abbott, R. Abbott, T. D. Abbott, F. Acernese, K. Ackley, C. Adams, T. Adams, P. Addesso, R. X. Adhikari, V. B. Adya *et al.*, Multi-messenger observations of a binary neutron star merger, *Astrophys. J.* **848**, L12 (2017).

[20] T. G. Cowling, The non-radial oscillations of polytropic stars, *Mon. Not. R. Astron. Soc.* **101**, 367 (1941).

[21] K. D. Kokkotas and B. G. Schmidt, Quasinormal modes of stars and black holes, *Liv. Rev. Relativ.* **2**, 2 (1999).

[22] K. S. Thorne and A. Campolattaro, Non-radial pulsation of general-relativistic stellar models. I. Analytic analysis for  $L \geq 2$ , *Astrophys. J.* **149**, 591 (1967).

[23] D. Radice, V. Morozova, A. Burrows, D. Vartanyan, and H. Nagakura, Characterizing the gravitational wave signal from core-collapse supernovae, *Astrophys. J.* **876**, L9 (2019).

[24] L. Keer and D. I. Jones, Developing a model for neutron star oscillations following starquakes, *Mon. Not. R. Astron. Soc.* **446**, 865 (2015).

[25] D. D. Doneva, E. Gaertig, K. D. Kokkotas, and C. Krüger, Gravitational wave asteroseismology of fast rotating neutron stars with realistic equations of state, *Phys. Rev. D* **88**, 044052 (2013).

[26] N. Stergioulas, A. Bauswein, K. Zagkouris, and H.-T. Janka, Gravitational waves and non-axisymmetric oscillation modes in mergers of compact object binaries, *Mon. Not. R. Astron. Soc.* **418**, 427 (2011).

[27] A. Bauswein and H.-T. Janka, Measuring Neutron-Star Properties via Gravitational Waves from Neutron-Star Mergers, *Phys. Rev. Lett.* **108**, 011101 (2012).

[28] K. Takami, L. Rezzolla, and L. Baiotti, Constraining the Equation of State of Neutron Stars from Binary Mergers, *Phys. Rev. Lett.* **113**, 091104 (2014).

[29] C. Chirenti, R. Gold, and M. C. Miller, Gravitational waves from f-modes excited by the inspiral of highly eccentric neutron star binaries, *Astrophys. J.* **837**, 67 (2017).

[30] J. Steinhoff, T. Hinderer, T. Dietrich, and F. Foucart, Spin effects on neutron star fundamental-mode dynamical tides: Phenomenology and comparison to numerical simulations, *Phys. Rev. Res.* **3**, 033129 (2021).

[31] T. K. Chan, Y.-H. Sham, P. T. Leung, and L.-M. Lin, Multipolar universal relations between  $f$ -mode frequency and tidal deformability of compact stars, *Phys. Rev. D* **90**, 124023 (2014).

[32] T. Hinderer, A. Taracchini, F. Foucart, A. Buonanno, J. Steinhoff, M. Duez, L. E. Kidder, H. P. Pfeiffer, M. A. Scheel, B. Szilagyi, K. Hotokezaka, K. Kyutoku, M. Shibata, and C. W. Carpenter, Effects of Neutron-Star Dynamic Tides on Gravitational Waveforms within the Effective-One-Body Approach, *Phys. Rev. Lett.* **116**, 181101 (2016).

[33] G. Pratten, P. Schmidt, and T. Hinderer, Gravitational-wave asteroseismology with fundamental modes from compact binary inspirals, *Nat. Commun.* **11**, 2553 (2020).

[34] N. Andersson and P. Pnigouras, The phenomenology of dynamical neutron star tides, *Mon. Not. R. Astron. Soc.* **503**, 533 (2021).

[35] C. Constantinou, S. Han, P. Jaikumar, and M. Prakash,  $g$ -modes of neutron stars with hadron-to-quark crossover transitions, *Phys. Rev. D* **104**, 123032 (2021).

[36] T. Zhao, C. Constantinou, P. Jaikumar, and M. Prakash, Quasi-normal  $g$ -modes of neutron stars with quarks, *Phys. Rev. D* **105**, 103025 (2022).

[37] N. Andersson and K. D. Kokkotas, Gravitational Waves and Pulsating Stars: What Can We Learn from Future Observations? *Phys. Rev. Lett.* **77**, 4134 (1996).

[38] N. Andersson and K. D. Kokkotas, Towards gravitational wave asteroseismology, *Mon. Not. R. Astron. Soc.* **299**, 1059 (1998).

[39] S. Jaiswal and D. Chatterjee, Constraining dense matter physics using f-mode oscillations in neutron stars, *Physics* **3**, 302 (2021).

[40] B. K. Pradhan and D. Chatterjee, Effect of hyperons on  $f$ -mode oscillations in neutron stars, *Phys. Rev. C* **103**, 035810 (2021).

[41] J. Schaffner and I. N. Mishustin, Hyperon-rich matter in neutron stars, *Phys. Rev. C* **53**, 1416 (1996).

[42] Particle Data Group, P. A. Zyla *et al.*, Review of particle physics, *Prog. Theor. Exp. Phys.* **2020**, 083C01 (2020).

[43] S. Weissenborn, D. Chatterjee, and J. Schaffner-Bielich, Hyperons and massive neutron stars: The role of hyperon potentials, *Nucl. Phys. A* **881**, 62 (2012).

[44] D. J. Millener, C. B. Dover, and A. Gal,  $\Lambda$ -nucleus single-particle potentials, *Phys. Rev. C* **38**, 2700 (1988).

[45] J. Schaffner, C. Greiner, and H. Stöcker, Metastable exotic multihypernuclear objects, *Phys. Rev. C* **46**, 322 (1992).

[46] J. Mareš, E. Friedman, A. Gal, and B. K. Jennings, Constraints on Sigma nucleus dynamics from Dirac phenomenology of Sigma-atoms, *Nucl. Phys. A* **594**, 311 (1995).

[47] J. Schaffner-Bielich and A. Gal, Properties of strange hadronic matter in bulk and in finite systems, *Phys. Rev. C* **62**, 034311 (2000).

[48] E. Friedman and A. GAL, In-medium nuclear interactions of low-energy hadrons, *Phys. Rep.* **452**, 89 (2007).

[49] T. Fukuda, A. Higashi, Y. Matsuyama, C. Nagoshi, J. Nakano, M. Sekimoto *et al.* (E224 Collaboration), Cascade hypernuclei in the  $(K^-, K^+)$  reaction on  $^{12}\text{C}$ , *Phys. Rev. C* **58**, 1306 (1998).

[50] P. Khaustov, D. E. Alburger, P. D. Barnes, B. Bassalleck, A. R. Berdoz, A. Biglan *et al.* (The AGS E885 Collaboration), Evidence of  $\Xi$  hypernuclear production in the  $^{12}\text{C}(K^-, K^+)^{12}\Xi$  reaction, *Phys. Rev. C* **61**, 054603 (2000).

[51] K. Yagi and N. Yunes, I-love-q relations in neutron stars and their applications to astrophysics, gravitational waves, and fundamental physics, *Phys. Rev. D* **88**, 023009 (2013).

[52] <https://dcc.ligo.org/LIGO-P1800115/public>.

[53] D. Alvarez-Castillo, A. Ayriyan, G. G. Barnaföldi, H. Grigorian, and P. Pósfay, Studying the parameters of the extended  $\sigma - \omega$  model for neutron star matter, *Eur. Phys. J.: Spec. Top.* **229**, 3615 (2020).

[54] I. F. Ranea-Sandoval, O. M. Guileira, M. Mariani, and M. G. Orsaria, Oscillation modes of hybrid stars within the relativistic cowling approximation, *J. Cosmol. Astropart. Phys.* **12** (2018) 031.

[55] C. V. Flores, Z. B. Hall, and P. Jaikumar, Nonradial oscillation modes of compact stars with a crust, *Phys. Rev. C* **96**, 065803 (2017).

[56] C. Chirenti, G. H. de Souza, and W. Kastaun, Fundamental oscillation modes of neutron stars: Validity of universal relations, *Phys. Rev. D* **91**, 044034 (2015).

[57] K. S. Thorne, Nonradial pulsation of general-relativistic stellar models. III. Analytic and numerical results for neutron stars, *Astrophys. J.* **158**, 1 (1969).

[58] S. Chandrasekhar and V. Ferrari, On the non-radial oscillations of a star, *Proc. R. Soc. Lond. A* **432**, 247 (1991).

[59] L. Lindblom and S. L. Detweiler, The quadrupole oscillations of neutron stars., *Astrophys. J.* **53**, 73 (1983).

[60] S. Detweiler and L. Lindblom, On the nonradial pulsations of general relativistic stellar models, *Astrophys. J.* **292**, 12 (1985).

[61] M. Leins, H. P. Nollert, and M. H. Soffel, Nonradial oscillations of neutron stars: A New branch of strongly damped normal modes, *Phys. Rev. D* **48**, 3467 (1993).

[62] H. Sotani, K. Tominaga, and K.-I. Maeda, Density discontinuity of a neutron star and gravitational waves, *Phys. Rev. D* **65**, 024010 (2001).

[63] C. J. Krüger, K. D. Kokkotas, P. Manoharan, and S. H. Völkel, Fast rotating neutron stars: Oscillations and instabilities, *Front. Astron. Space Sci.* **8**, 166 (2021).

[64] H.-J. Kuan and K. D. Kokkotas,  $f$ -mode imprints in gravitational waves from coalescing binaries involving spinning neutron stars, [arXiv:2205.01705](https://arxiv.org/abs/2205.01705).

[65] L. Tonetto, A. Sabatucci, and O. Benhar, Impact of three-nucleon forces on gravitational wave emission from neutron stars, *Phys. Rev. D* **104**, 083034 (2021).

[66] F. J. Zerilli, Effective Potential for Even-Parity Regge-Wheeler Gravitational Perturbation Equations, *Phys. Rev. Lett.* **24**, 737 (1970).

[67] E. D. Fackerell, Solutions of Zerilli's equation for even-parity gravitational perturbations, *Astrophys. J.* **166**, 197 (1971).

[68] O. Benhar, V. Ferrari, and L. Gualtieri, Gravitational wave asteroseismology reexamined, *Phys. Rev. D* **70**, 124015 (2004).

[69] J. L. Blázquez-Salcedo, L. M. González-Romero, and F. Navarro-Lérida, Polar quasi-normal modes of neutron stars with equations of state satisfying the  $2 m_\odot$  constraint, *Phys. Rev. D* **89**, 044006 (2014).

[70] D.-H. Wen, B.-A. Li, H.-Y. Chen, and N.-B. Zhang, Gw170817 implications on the frequency and damping time of *f*-mode oscillations of neutron stars, *Phys. Rev. C* **99**, 045806 (2019).

[71] K. Kokkotas (private communication).

[72] L. K. Tsui and P. T. Leung, Universality in quasi-normal modes of neutron stars, *Mon. Not. R. Astron. Soc.* **357**, 1029 (2005).

[73] G. Lioutas and N. Stergioulas, Universal and approximate relations for the gravitational-wave damping timescale of *f*-modes in neutron stars, *Gen. Relativ. Gravit.* **50**, 12 (2018).

[74] J. S. Read, L. Baiotti, J. D. E. Creighton, J. L. Friedman, B. Giacomazzo, K. Kyutoku, C. Markakis, L. Rezzolla, M. Shibata, and K. Taniguchi, Matter effects on binary neutron star waveforms, *Phys. Rev. D* **88**, 044042 (2013).

[75] S. Bernuzzi, T. Dietrich, and A. Nagar, Modeling the Complete Gravitational Wave Spectrum of Neutron Star Mergers, *Phys. Rev. Lett.* **115**, 091101 (2015).

[76] S. Vretinaris, N. Stergioulas, and A. Bauswein, Empirical relations for gravitational-wave asteroseismology of binary neutron star mergers, *Phys. Rev. D* **101**, 084039 (2020).

[77] S. Blacker, Niels-Uwe F. Bastian, A. Bauswein, D. B. Blaschke, T. Fischer, M. Oertel, T. Soulantasis, and S. Typel, Constraining the onset density of the hadron-quark phase transition with gravitational-wave observations, *Phys. Rev. D* **102**, 123023 (2020).

[78] K. Chakravarti and N. Andersson, Exploring universality in neutron star mergers, *Mon. Not. R. Astron. Soc.* **497**, 5480 (2020).

[79] K. D. Kokkotas, T. A. Apostolatos, and N. Andersson, The inverse problem for pulsating neutron stars: A 'fingerprint analysis' for the supranuclear equation of state, *Mon. Not. R. Astron. Soc.* **320**, 307 (2001).

[80] H. Sotani and B. Kumar, Universal relations between the quasi-normal modes of neutron star and tidal deformability, *Phys. Rev. D* **104**, 123002 (2021).

[81] W. Kirch, ed., Pearson's correlation coefficient, in *Encyclopedia of Public Health* (Springer Netherlands, Dordrecht, 2008), pp. 1090–1091.

[82] S. Yoshida and Y. Eriguchi, Neutral points of oscillation modes along equilibrium sequences of rapidly rotating polytropes in general relativity: Application of the cowling approximation, *Astrophys. J.* **490**, 779 (1997).

[83] C. V. Flores and G. Lugones, Discriminating hadronic and quark stars through gravitational waves of fluid pulsation modes, *Class. Quant. Grav.* **31**, 155002 (2014).

[84] D. Kumar, H. Mishra, and T. Malik, Non-radial oscillation modes in hybrid stars: Consequences of a mixed phase, [arXiv:2110.00324](https://arxiv.org/abs/2110.00324) [hep-ph].

[85] H. C. Das, A. Kumar, S. K. Biswal, and S. K. Patra, Impacts of dark matter on the *f*-mode oscillation of hyperon star, *Phys. Rev. D* **104**, 123006 (2021).

[86] S. Shashank, F. H. Nouri, and A. Gupta, *f*-mode oscillations of compact stars in dynamical spacetimes: Equation of state dependencies and universal relations studies, [arXiv:2108.04643](https://arxiv.org/abs/2108.04643) [gr-qc].

[87] T. Zhao and J. M. Lattimer, Universal relations for neutron star *F*-mode and *G*-mode oscillations, [arXiv:2204.03037](https://arxiv.org/abs/2204.03037).

[88] X. Mu, B. Hong, X. Zhou, G. He, and Z. Feng, The influence of entropy and neutrinos on the properties of protoneutron stars, *Eur. Phys. J. A* **58**, 76 (2022).

[89] P. Schmidt and T. Hinderer, Frequency domain model of *f*-mode dynamic tides in gravitational waveforms from compact binary inspirals, *Phys. Rev. D* **100**, 021501(R) (2019).

[90] L. Gualtieri, E. M. Kantor, M. E. Gusakov, and A. I. Chugunov, Quasinormal modes of superfluid neutron stars, *Phys. Rev. D* **90**, 024010 (2014).

[91] W. C. G. Ho, D. I. Jones, N. Andersson, and C. M. Espinoza, Gravitational waves from transient neutron star *f*-mode oscillations, *Phys. Rev. D* **101**, 103009 (2020).

[92] G. A. *et al.*, Bilby: A user-friendly bayesian inference library for gravitational-wave astronomy, *Astrophys. J. Suppl. Ser.* **241**, 27 (2019).

[93] B. P. Abbott *et al.* (KAGRA, LIGO Scientific, and Virgo Collaboration), Prospects for observing and localizing gravitational-wave transients with Advanced LIGO, Advanced Virgo and KAGRA, *Living Rev. Relativ.* **21**, 3 (2018).

[94] <https://dcc.ligo.org/LIGO-T2000012/public>.

[95] S. H. *et al.*, Sensitivity studies for third-generation gravitational wave observatories, *Class. Quant. Grav.* **28**, 094013 (2011).

[96] <https://dcc.ligo.org/LIGO-T1500293/public>.